ADVANCED OPTICAL MATERIALS
www.advopticalmat.de

Noble Metal Coating on Perovskite Microcrystals for Robust and Plasmonic Lasing Applications

*Sangyeon Cho, Hao Yan, and Seok Hyun Yun**

Lead halide perovskites (LHP) are solution-processable semiconductor materials with high optical gain and broad wavelength tunability, making them well-suited for laser applications. Here, a solution-based method for the 3D conformal coating of LHP microcrystals with noble metals is presented. A nanoscale metal coating layer is found to significantly enhance both laser performance and environmental stability. This enables gold-coated $CsPbBr_3$ microcrystals to be delivered into live cells, achieving single-mode plasmonic lasing under optical pumping. Silver-coated $CsPbBr_3$ particles demonstrate stable plasmonic lasing in the air. This one-pot synthesis method opens new possibilities for leveraging LHPs to implant micro-laser sources into physical, biological, and industrial systems.

1. Introduction

Micro- and nanocrystals of lead halide perovskites (LHPs) have received significant attention for their applications in light-emitting diodes (LEDs)[1] and photovoltaic devices.[2] Their low-cost solution processibility, broad bandgap tunability, and high optical gain also make them attractive for miniature lasers.[3–9] Recently, substrate-less micro- and nano-lasers in the form of particles—termed laser particles (LPs)— have been developed,[10–14] addressing applications that conventional bulky or on-chip lasers cannot serve for. For example, micro- or nano-LPs can be implanted into materials or integrated into biological systems, such as living cells. Traditionally, these LPs have been fabricated using III–V semiconductor gain materials through top-down fabrication techniques. LHPs offer a distinctive bottom-up approach, enabling the synthesis of micro- and nanocrystals via a solution-based method.[15,16]

In addition to semiconductor gain materials, incorporating noble metals into laser resonators has proven to be an effective approach for miniaturizing laser dimensions through the plasmon-enhanced Purcell effects.[17–22] For example, plasmonic LPs using III–V disk particles coated with gold have demonstrated significant size reductions to subwavelength dimensions.[14] This plasmonic Purcell effect enhances optical gain sufficiently to offset metallic losses. The plasmonic effect with LHPs has previously been explored using $CsPbBr_3$ particles placed on gold[9] or silver substrates.[23] However, achieving substrate-free plasmonic LPs based on LHPs is challenging, as it requires effective methods for integrating noble metals directly onto LHP particles.

Previously, noble metal coatings on III–V and II–VI semiconductors were achieved using various fabrication methods, including electron-beam deposition,[14,21] electroplating,[24–26] and reduction chemistry.[27–29] While electron-beam deposition and electroplating are well established for on-chip devices, they often result in numerous grain boundaries at thin gold thicknesses.[30] Moreover, lifting particles off the substrate after deposition presents significant challenges. These methods are therefore not well-suited for metal coating on LHP particles. In contrast, reduction chemistry offers a viable approach for achieving thin, conformal metal coatings on nanomaterials in solutions. However, applying conventional reduction chemistry to LHPs is challenging due to undesired side reactions, such as galvanic displacement[31,32] of noble metal ions and halide anion exchange.[33,34] Furthermore, the rapid dissolution of LHPs in water and their low thermal stability[35–38] hinder the direct use of traditional noble metal reduction.

Here, we present a novel reduction chemistry method for the one-pot synthesis of metal-coated LHP micro- and submicron-crystals capable of lasing.[39] We demonstrate gold and silver coating on $CsPbBr_3$ microcrystals with minimal material degradation[40–45] or phase transformation[46] during the coating process. These particles exhibit lasing under optical pumping, producing narrowband single-mode spectra. Notably, the gold coating significantly improves environmental stability by protecting the particles against humidity, resulting in robust lasing performance.[35–38] Additionally, the gold surface facilitates functionalization with biomaterials such as proteins and liposomes. This capability enabled the intracellular delivery of $CsPbBr_3$

S. Cho, H. Yan[+], S. H. Yun
Harvard Medical School and Wellman Center for Photomedicine
Massachusetts General Hospital
Cambridge, MA 02139, USA
E-mail: syun@hms.harvard.edu
S. H. Yun
Harvard-MIT Health Sciences and Technology
Massachusetts Institute of Technology
Cambridge, MA 02139, USA

The ORCID identification number(s) for the author(s) of this article can be found under https://doi.org/10.1002/adom.202403316

[+]Present address: Tsinghua Shenzhen International Graduate School, Tsinghua University, Shenzhen 518055, China

DOI: 10.1002/adom.202403316

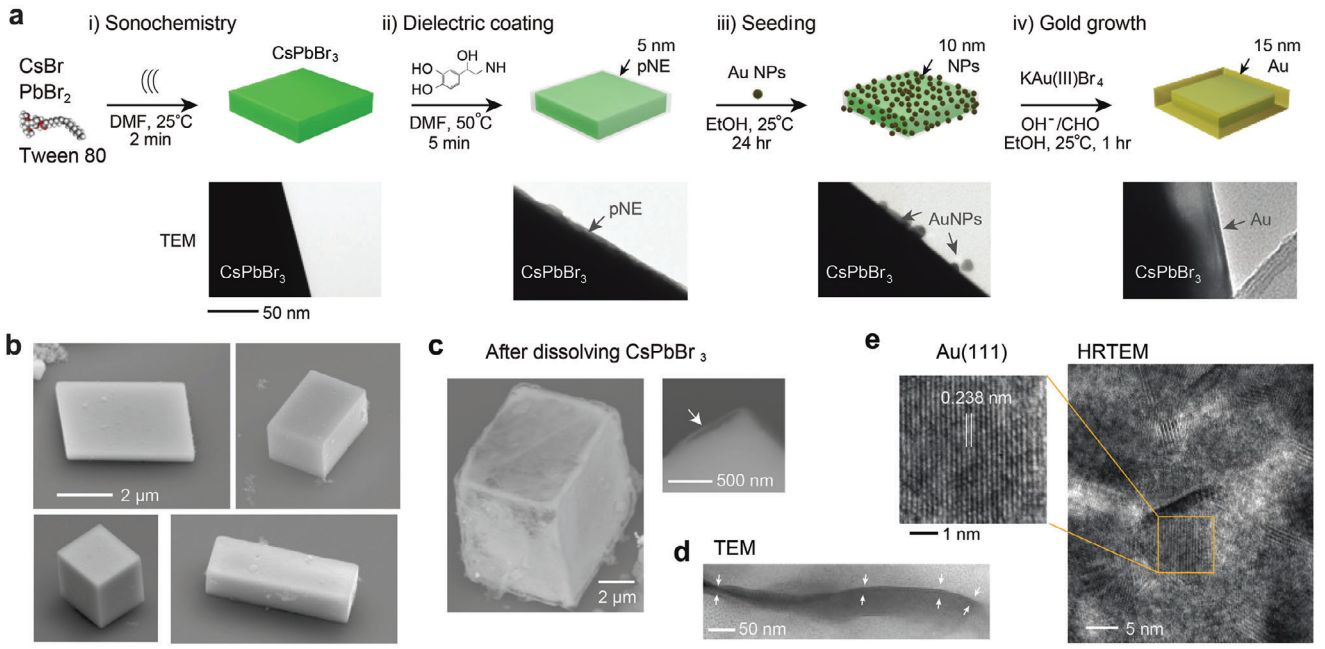

Figure 1. Synthesis of gold-coated perovskite particles. a) Schematic illustration of the sequential steps in the synthesis of gold coated $CsPbBr_3$ particles (top) with corresponding representative TEM images captured at the conclusion of each step (bottom). b) SEM images showcasing gold-coated $CsPbBr_3$ particles with various aspect ratios. c) SEM images displaying the gold/pNE coating ≈20 nm in thickness on core–shell particles, illustrating conditions of (left) complete and (right) partial dissolution of the $CsPbBr_3$ core. d) TEM image depicting the 5 nm-thick pNE coating layer. e) High-resolution TEM image of the gold coating layer, exhibiting polycrystalline domains. An inset highlights a region showing the characteristic (111) plane of gold a fringe spacing of 0.238 nm.

microparticles into live cells, where optically pumped lasing was achieved within the cytoplasm.

2. Results

2.1. Synthesis and Structural Characterization of Gold Coated $CsPbBr_3$ Particles

Previously, we developed a sonochemistry method to generate $CsPbBr_3$ microcrystals in polar aprotic N,N-dimethylformamide (DMF) solvent and subsequently coated them with polynorepinephrine (pNE) in a saturated condition created by sonochemistry.[47,48] In this research, we utilized pNE layers to capture both metal nanoparticle seeds and metal ions.[28,29] Our method transforms metal ions into metal films using reducing agents in ethanol under alkaline conditions. By preserving the quality of $CsPbBr_3$ during the redox process,[49] this method culminates in a conformal, optically thin layer of gold or silver that envelops the insulated surfaces of the $CsPbBr_3$ particles.

Figure 1a illustrates this novel coating method in four distinct steps: i) sonochemical synthesis of all inorganic $CsPbBr_3$ microcrystals, ii) application of a pNE dielectric coating in a saturated $CsPbBr_3$ solution, iii) seeding of gold nanoparticle, and iv) growth of a thin gold film (See Experimental Section and Supporting Information). Transmission electron micrography (TEM) captured the stepwise evolution of the $CsPbBr_3$ particle surface (Figure 1a). Initially, sonochemistry facilitated the crystallization of orthorhombic $CsPbBr_3$ microcrystals within a DMF solution laden with precursors at their saturated point. The addition of a nonionic surfactant, Tween 80, aids in modulating the aspect ratio of $CsPbBr_3$ microcrystals toward plate-like configurations.[47] Despite the general susceptibility of $CsPbBr_3$ to polar solvents, the saturated DMF solution stabilized the particles, enabling subsequent surface coating with self-polymerizable norepinephrine without disturbing the saturation conditions.[48]

A conformal pNE coating, ≈5 nm thick, was then applied, providing organic functional groups for the attachment of 10 nm-sized gold nanoparticles used in seeding.[28,29] Without the pNE coating, gold seeds may attach to the bare surface of $CsPbBr_3$ particles but fail to form a conformal gold film (Figure S1, Supporting Information). The pNE layer also played a crucial role as an insulating gap, preventing charge carrier quenching during laser operation. Gold (III) ions, supplied by $KAuBr_4$, facilitated this process while avoiding undesirable anion exchange of the $CsPbBr_3$ perovskite.[33,34] The final step involved the reduction of gold ions through the electrocatalytic oxidation of ethanol with formaldehyde in alkaline conditions, producing a conformal polycrystalline gold film atop the pNE layer.[49] The use of larger gold nanoparticles (50 nm diameter) resulted in increased metal surface roughness (Figure S2a, Supporting Information). Increasing the concentration of formaldehyde and NaOH increased the gold thickness (Figure S2b, Supporting Information). The target thickness of the gold coating was ≈15 nm, optimized to permit optical pumping and laser light emission through the metal layer.

Scanning electron micrography (SEM) analysis of the resulting gold-coated $CsPbBr_3$ microparticles revealed excellent structural integrity with no noticeable damage (Figure 1b). These

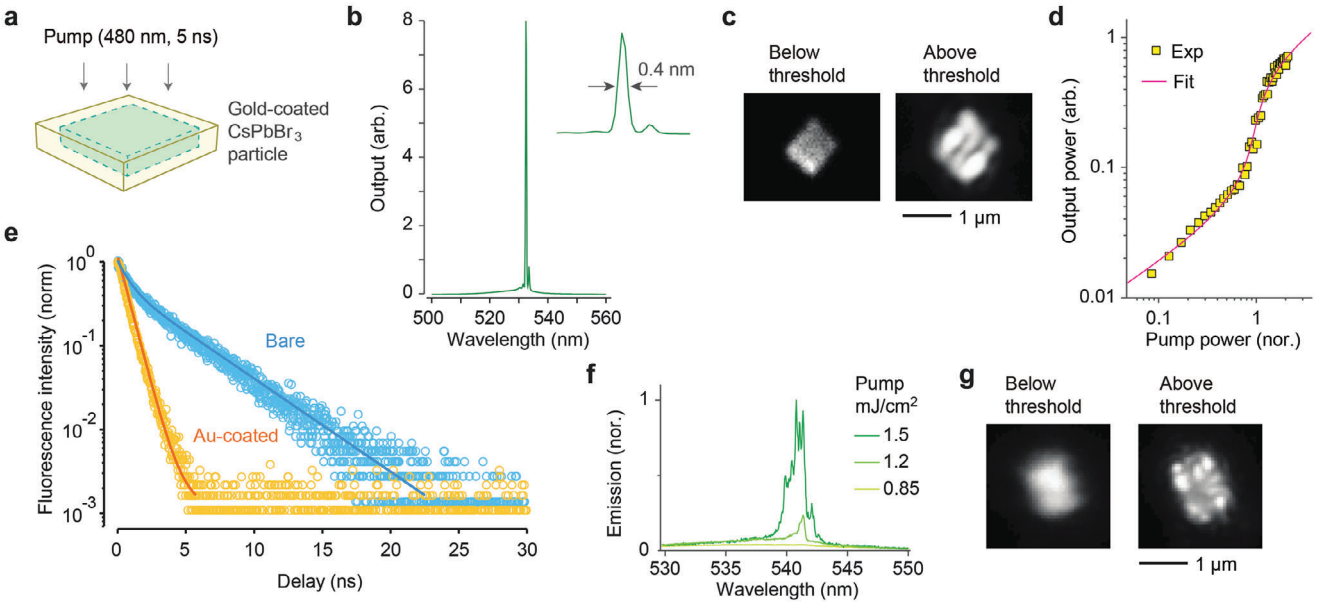

Figure 2. Optical characteristics of gold-coated $CsPbBr_3$ particles. a) Schematic depicting the process of optical pumping. b) Emission spectrum obtained from a particle-sized 2 μm under a pump fluence of 1.2 mJ cm^{-2}. Inset shows a detailed zoom of the spectrum. c) Wide-field images of the output emission from a gold-coated $CsPbBr_3$ below and above lasing threshold (threshold pump fluence: 0.8 mJ cm^{-2}). d) Measured output power (squares) and a theoretical fitting curve. e) Fluorescence decay curves for both gold-coated and uncoated particles (four samples each, sized ≈1.8 μm × 1.8 μm × 0.25 μm). Curves are fitted using a double-exponential model. f) Spectra illustrating random lasing of a particle not coated with pNE but attached to gold seed nanoparticles, observed at three different pump levels: 0.85, 1.2, and 1.5 mJ cm^{-2}. g) Wide-field emission images from a gold nanoparticle-coated $CsPbBr_3$ sample fabricated without pNE coating, below and lasing (threshold pump fluence: 1 mJ cm^{-2}). The bright spots in the above-threshold image are due to light scattering from AuNPs on the surface.

particles retained their structural integrity in water for 1–2 h before the $CsPbBr_3$ cores dissolved after extended water exposure, leaving behind the metal layer structure (Figure 1c). This finding indicates a 3- to 6-fold improvement in lifetime in water compared to pNE-only coated $CsPbBr_3$ microparticles, and it represents a four-order-of-magnitude improvement compared to bare particles.[48] Further characterizations after dissolution revealed the combined gold/pNE layer to be ≈20 nm thick (Figure 1c), with the gold layer itself measuring ≈15 nm, as the pNE coating was initially 5 nm (Figure 1d). High-resolution TEM images confirmed the polycrystalline nature of the gold film, with lattice fringe patterns indicative of the gold (111) plane, measuring a periodicity of 2.38 Å (Figure 1e; Figure S3, Supporting Information).

2.2. Lasing Characterization of Gold Coated $CsPbBr_3$ Particles in Air

We measured the lasing characteristics of gold-coated $CsPbBr_3$ particles under ambient room conditions (**Figure 2a**) using a custom-built microscope setup, which included a grating-based spectrometer with a spectral resolution of 0.2 nm (Figure S4, Supporting Information). The excitation source consisted of nanosecond pulses from an optical parametric oscillator, tuned to 480 nm. A representative emission spectrum from a gold-coated particle, measuring 2 μm in side-length and 0.2 μm in height, dispersed on a thermal oxide silicon substrate, is presented in Figure 2b. This was obtained at a pump fluence of 1.2 mJ cm^{-2}, above a lasing threshold at 0.8 mJ cm^{-2}, or 1.6 mW μm^{-2} in peak power, showing a single-mode peak with a linewidth of 0.4 nm and a minor sidelobe. Notably, the low fluorescence background above lasing threshold was significantly lower than that usually seen in similar-sized, non-gold-coated $CsPbBr_3$ particles.[9] Wide-field images of the output emission present distinct mode patterns above the threshold (Figure 2c). The light-in-light-out curve, shown in Figure 2d, exhibits a characteristic nonlinear increase at the threshold, marked by a kink parameter of 0.04. It is estimated that the 15 nm gold layer absorbs ≈50% of pump light.[49] Thicker gold thickness results in excessive pump loss, as well as attenuation of light emitted from the core. We did not observe lasing from samples fabricated with 50 nm gold nanoparticles (Figure S2, Supporting Information).

Time-resolved photoluminescence spectroscopy demonstrated a significant reduction in the fluorescence decay times of gold-coated $CsPbBr_3$ particles compared to their uncoated counterparts (Figure 2e). The decay parameters, determined via bi-exponential fitting, are summarized in Table S1 (Supporting Information). Furthermore, finite-difference time-domain (FDTD) simulations identified photonic-plasmonic hybrid modes within gold-coated particle models, characterized by a quality (Q) factor of ≈120 and a Purcell factor of 4 (Figure S5, Supporting Information). The observed decrease in the radiative emission lifetime from 123 ns in uncoated samples to 22.5 ns can be primarily attributed to the moderate Purcell effect, which enhances both spontaneous and stimulated emission rates during laser oscillation. Stronger Purcell factors have been measured in submicron-sized particles in air.[9,49] However, for

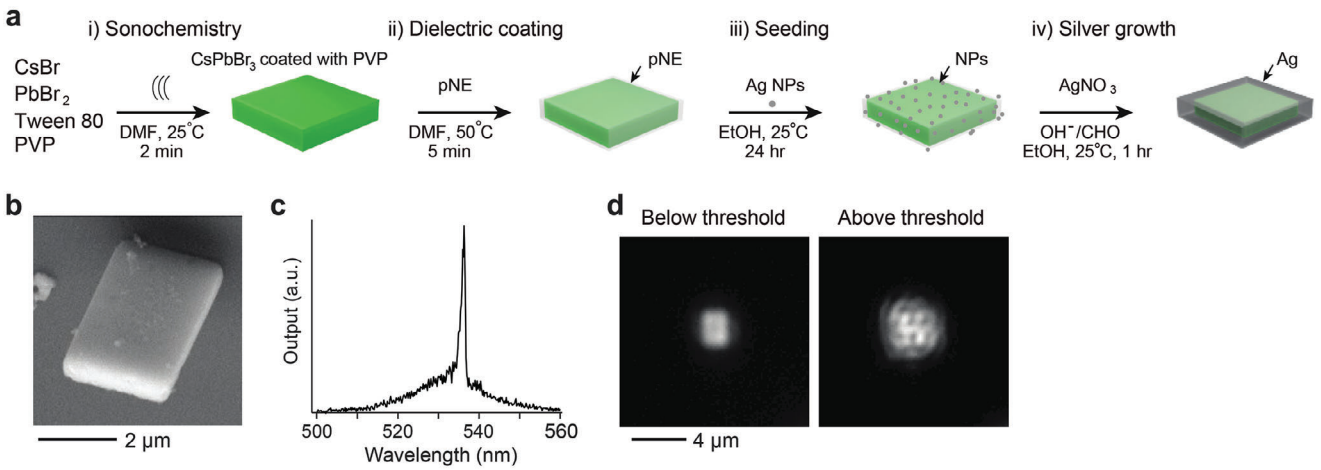

Figure 3. Silver-coated $CsPbBr_3$ particles. a) Schematic illustrating the sequence of steps for applying a silver coating. The application of an initial polyvinylpyrrolidone (PVP) layer as a dielectric insulator is critical for maintaining stable photoluminescence. b) SEM image showcasing a silver coated $CsPbBr_3$ particle. c) Emission spectrum from a 2.4-μm-sized, silver-coated particle at a pump fluence of 1.5 mJ cm^{-2}. d) Far-field emission profiles illustrating the transition below and above the lasing threshold.

operation in water, higher Q factors in micron-sized particles are more advantageous. The optical characteristics of microparticles were largely insensitive to the particle size in a size range from one to a few microns.

Intriguingly, a subset of exploratory samples fabricated without the pNE coating step demonstrated the ability to produce lasing with relatively broad, multi-peak spectra (Figure 2f). This output characteristic is indicative of plasmonic scattering-assisted random lasing phenomena.[50,51] Optical imaging of these particles confirmed the presence of numerous discrete gold seed nanoparticles on the $CsPbBr_3$ surface (Figure 2g).

2.3. Silver Coated $CsPbBr_3$ Particles

Silver has lower loss than gold for plasmonic polariton guidance in the $CsPbBr_3$ emission spectral range. We investigated the feasibility of silver coating on $CsPbBr_3$. Our approach to achieving conformal silver coating involves the use of 10 nm-sized silver seed nanoparticles and silver nitrate ($AgNO_3$) as the source of Ag (I) ions (**Figure 3a**). A key distinction from the aforementioned gold coating methodology is the incorporation of a nonionic polymeric surfactant, specifically polyvinylpyrrolidone (PVP), during the sonochemical synthesis of the $CsPbBr_3$ particles. This surfactant creates a thin encapsulating layer, a few nanometers thick, around the $CsPbBr_3$ cores, acting as a dielectric energy barrier. This barrier is crucial for reducing undesirable transport and quenching of photo-induced charges between the $CsPbBr_3$ cores and the surrounding pNE and silver layers during laser oscillation. TEM images visualized the high surface quality of the silver-coated $CsPbBr_3$ particles, showing no significant damage (Figure 3b). Upon optical pumping with fluences exceeding 1 mJ cm^{-2}, we observed single-peak laser emission in air (Figure 3c). The far-field emission profiles, particularly above the lasing threshold, displayed symmetric interference patterns indicative of narrowband laser emissions (Figure 3d).

2.4. Lasing Stability of Noble-Metal-Coated $CsPbBr_3$ Particles

The absence of a PVP layer in silver coating led to rapid degradation of the silver-coated particles upon photoexcitation (**Figure 4a**). This is attributed to the ability of Ag^+ ions to penetrate the pNE layer and directly interact with the catechol groups of pNE,[52] causing quenching of the photo-induced charges from the $CsPbBr_3$ core. Recent ultrafast spectroscopy studies revealed that non-fluorescent recombination occurs through charge-separated states, via plasmon-induced hot-electron transfer from the metal to the semiconductor, or through plasmons directly damping to form charge-separated electrons and holes at the interface.[53] In contrast, the gold coating process does not necessitate a PVP barrier since Au^{3+} ions tend to coordinate with the outer surface of the pNE layer rather than penetrating it. Time-lapse recordings of the output spectra confirmed the stability of the PVP-protected silver-coated particles under continuous pumping (Figure 4b). PVP provided the greatest stability among various polymers we evaluated, including polyhedral oligomeric silsesquioxane (POSS) (Figure 4c). While stable in air, however, the silver-coated particles immersed in water survived only briefly, less than 10 min, before they lost photoluminescence functionality. Further optimization of charge-insulating barriers or adding an additional dielectric shell on top of the silver coating may extend the lifespan.

For gold-coated particles, we observed no significant shift (<0.02 nm) in the emission wavelengths during continuous optical pumping at 20 Hz for 500 s (equating to 10 000 pump pulses) (Figure 4d). A slight reduction in output intensity, ranging from 5% to 10%, was observed, suggesting photo-induced aging during the active operation. Notably, the fluctuations in both lasing peak wavelength and intensity from pulse to pulse were 2- to 3-fold lower than uncoated particles. This enhanced stability is possibly due to diminished charge accumulation at the heterojunction interface and reduced exposure to atmospheric oxygen.[54] Due to the superior stability of gold-coated particles compared to

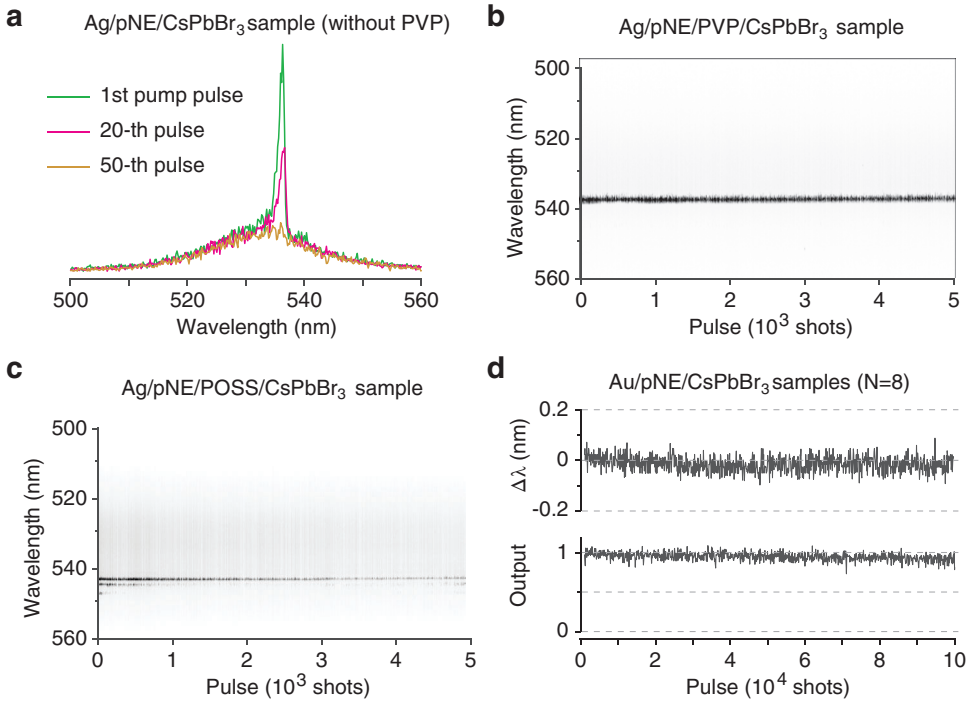

Figure 4. Laser stability in air. a) Single-shot output spectra of a silver-coated $CsPbBr_3$ particle (2.9 μm in size) fabricated without PVP layers, showing the rapid degradation of the perovskite upon successive pump pulses. b) Output spectra of a PVP-incorporated silver-coated $CsPbBr_3$ particle, showing stability over an extended exposure to pulsed pumping. c) Output spectra from a POSS-incorporated silver-coated sample. Intensities of the spectral traces in (b,c) represent output intensity. d) Graphs showing the stability of the lasing peak wavelength (top) and intensity (bottom) across 10 000 pumping pulses, with plotted traces representing the average from eight gold coated $CsPbBr_3$ samples. All these measurements used a pump pulse fluence of 1.5 mJ cm^{-2}.

silver-coated particles in water, we opted to use gold-coated particles for intracellular applications.

2.5. Functionalization and Robust Plasmonic Lasing of Gold-Coated $CsPbBr_3$ in Water

The enhanced stability of the gold-coated $CsPbBr_3$ particles in aqueous environments, coupled with their gold surfaces, facilitated versatile functionalization through various physical and chemical methods. These methods enable the attachment of diverse materials, including polystyrene, liposomes, quantum dots, and fluorescent proteins (**Figure 5**a; Experimental Section). For instance, sulfur (—SH) groups present on gold surfaces can form covalent bonds with amine ($—NH_2$) groups through a simple one-step mixing reaction in water. This approach was utilized to attach DsRed fluorescent proteins and CdSe quantum dots to the particles. Furthermore, incorporating the particles into large liposomes of DIR dye-labeled, 1,2-dioleoyl-sn-glycero-3-phosphoethanolamine (DOPE) and 1, 2-dioleoyl-3-trimethylammonium-propane (DOTAP) resulted in

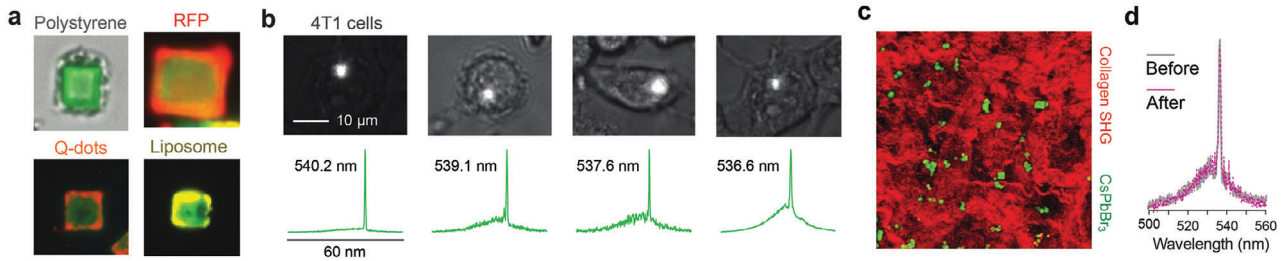

Figure 5. Functionalization and biological application of gold-coated $CsPbBr_3$ particles. a) Fluorescence microscopy images showcasing gold-coated $CsPbBr_3$ particles (emitting green fluorescence) interfaced with various materials, including polystyrene (appearing gray), dye-conjugated liposomes (yellow), CdS/CdSe quantum dots (orange), and red fluorescent proteins (red). b) (Top) Bright-field images of four live 4T1 cells with gold-coated $CsPbBr_3$ particles (visible as bright spots) with their cytoplasm under optical excitation. (Bottom) Emission spectra from these cells. c) Two-photon excited fluorescence microscopy image of $CsPbBr_3$ particles (green) injected into porcine sclera tissue. Red: second-harmonic generation signals from collagen fibers. d) Single-shot emission spectra of a gold-coated $CsPbBr_3$ particle embedded in the tissue, before and after two-photon microscopy (≈10^{10} femtosecond pulses), demonstrating stability.

their liposomal encapsulation, enhancing their delivery into cells in vitro (Figure S6, Supporting Information). Previously, attempts to observe lasing with liposome-encapsulated, pNE-only coated $CsPbBr_3$ particles delivered into cells was unsuccessful.[48] However, the augmented stability afforded by the gold coating enabled us to achieve intracellular lasing within live 4T1 breast cancer cells for the first time (Figure 5b). The average threshold fluence for inducing lasing in intracellular particles was found to be 0.83 mJ cm^{-2}. The estimated lifetime of gold-coated particles within the cytoplasm extended to ≈2 h, likely due to the formation of a protective protein corona around the particle surfaces, slightly improving their lifespan compared to their stability in water. When injected into hydrated porcine sclera tissue ex vivo, the gold-coated $CsPbBr_3$ particles demonstrated their ability to lase under separate OPO pumping (480 nm, 20 Hz), enduring the femtosecond laser pulses (≈150 fs, 100 pJ, 80 MHz, 920 nm) employed in two-photon microscopy without degradation (Figure 5c,d).[55] While the pump levels of a few mJ cm^{-2}, corresponding to several pJ per pulse, are higher than those in other low-threshold laser systems, the energy per pulse at a 20 Hz repetition rate is considered suitable for biological applications due to sufficient cooling time between pulses. For example, considering the skin tissue exposure limit[56] of ≈0.25 J cm^{-2}, pulse repetition rates up to 100 kHz could be acceptable for exposure times of up to 1 ms. Therefore, these results demonstrate the potential of these gold-coated LPs for biological applications.

3. Conclusion

Three distinct strategies have been exploited to improve the stability of LHP-based micro- and nanoparticles. First, sealing entire substrate-based devices through physical deposition has proven effective for on-chip applications[57,58] but is not readily applicable to substrate-free LPs. Second, coating LHP nanocrystals with oxide or semiconductor shells, such as SiO_2,[40–42] ZrO_2,[43] TiO_2,[45] and CdS,[44] has been shown to enhance stability. However, these methods often degrade optical properties due to adverse synthesis conditions, including polar precursors, hydrolytic byproducts, high-temperature calcification, and interfacial charge transfer. Also, water-triggered transformation forming a Cs_4PbBr_6 endotaxy shell has been observed to reduce optical gain.[46] Third, embedding LHP nanocrystals in polymeric matrices,[59] polystyrene microbeads,[60] or long-chain lipid shells[61–63] offers environmental stability. However, this approach is challenging to extend to microparticles with larger surface areas due to the thermodynamics of surface ligand exchange.

The conformal metal coating approach presented here provides significant advantages. It utilizes a facile one-pot process, minimally increases particle size, enhances environmental stability, and introduces plasmonic effects. Currently, the operational lifetime of gold-coated $CsPbBr_3$ microparticles in aqueous environments is a few hours (see Table S2, Supporting Information). While this duration suffices for surface functionalization and proof-of-concept experiments in cellular and tissue contexts, further improvements are needed for practical applications.[10–14] Extending stability beyond several hours for short-term assays[18] and a few days for long-term studies[14] is critical. Optimizing the coating process offers a promising route toward enhanced stability. For example, a single-crystalline gold coating could be grown on polydopamine-coated LHPs using an ethylene glycol/water interface,[64] while an alternative silver coating may be achieved through Tollens' reagent.[65] A hybrid method, combining seeding with electron-beam lithography at the nanoscale with subsequent reduction reactions, could minimize grain boundaries and enhance surface smoothness.

One notable drawback of LHPs for biological applications is the presence of lead (Pb). Lead ion concentrations as low as 10 µM have been associated with elevated cytokine production in human PBMC cells.[66] Higher concentrations, ranging from 0.1 to 1 mM, corresponding to LC50 (Lethal Concentration for 50% of the population) and EC50 (Effective Concentration for 50% of the population) levels.[67] However, intracellular LHP nanoparticles encapsulated in thick polymer beads have demonstrated ≈100% viability in macrophage (RAW 264.7) cells over a 24 h period.[60] Metal-coated LHP LPs may be suitable for specific assays where potential lead toxicity has minimal impact.

Lead-free tin halide perovskites exhibit reduced toxicity in vivo.[67–70] While their water solubility is generally higher than that of LHPs,[71] the incorporation of quasi-1D, 2D, or 2D/3D tin perovskite structures with organic spacers has shown enhanced moisture stability.[72–75] Additionally, conformal metal coating can be applied to tin halide perovskites to further improve their stability and mitigate toxicity.

Beyond biological applications, the metal coating technique holds potential for improving the performance of various LHP-based devices, including LEDs,[76] solar cells,[35] and non-blinking quantum dots,[28] 3D laser-printed quantum dots,[77,78] and low-dimensional Ruddlesden–Popper perovskites.[79,80] The accelerated dynamics of plasmonic lasing also enable sub-picosecond pulses[81] which are useful for high-bandwidth optical communications and quantum imaging. Furthermore, metal-LHP particles may serve as platforms for exploring fundamental phenomena, such as exciton-polariton strong coupling,[82] plasmonic nonlocal effects,[83] and plasmonic hinge modes.[39]

4. Experimental Section

Materials: CsBr (99.99%), $PbBr_2$ (99.99%), NaOH (Pallets), NaOH (solution) (±)-norepinephrine (+)-bitartrate salt, N,N dimethylformamide (anhydrous, 99.8%), $KAuBr_4$, formaldehyde, ethanol (anhydrous, ≥99.5%) were purchased from Sigma–Aldrich. Au nanoparticles were purchased from Nanocomposix. 1,2-dioleoyl-sn-glycero-3-phosphoethanolamine (DOPE) and 1,2-dioleoyl-3-trimethylammonium-propane (DOTAP) were purchased from Avanti polar lipid. DiIC18 (1,1′-Dioctadecyl-3,3,3′,3′-Tetramethylindotricarbocyanine Iodide) dye (DIR), proLong gold antifade mountant with 4,6-diamidino-2-phenylindole (DAPI) were purchased from Thermo Scientific. rDSRed-express protein was purchased from Takara Bio. All reagents were used as received without further purification.

Synthesis Method: The fabrication of $CsPbBr_3$/pNE/Au particles was a four-step procedure:

Step 1) Sonocrystallization: 75 mM of each CsBr and $PbBr_2$ salts were dispersed at an equal concentration in 1 mL of N,N-dimethylformamide (DMF) in a glass vial. 1 µL of TWEEN 80 was added into the solution. The role of non-ionic surfactant was to help to generate $CsPbBr_3$ particles with different size aspect ratio. The vial was placed into a bath-type ultrasonicator (Elmasonic P60H, Elma) at 80 kHz in room temperature and irradiated with ultrasonic waves at a frequency of 80 kHz. After 2–3 min of ultrasonication, $CsPbBr_3$ micro- and submicron-sized crystals were spontaneously

crystallized and dispersed in the solution. The saturated condition prevented the dissolution of the $CsPbBr_3$ particles in polar aprotic DMF and allows for the subsequent coating with amphiphilic polymers.

Step 2) Dielectric coating: Catechol amine molecules including dopamine or norepinephrine could generate self-polymerization on various surfaces. The coating solution was prepared by simply dissolving 4 mg of (±)-norepinephrine (+)-bitartrate salt and a pallet of NaOH into 1 mL of the supernatant of the sonochemical reaction of $CsPbBr_3$ or the saturated DMF solution. The undissolved NaOH pallet was discarded. The vial with an untightened cap was shaken at 1000 rpm at 25 °C for 5 min to construct poly-norepinephrine (pNE) coating with 5 nm. After the product was centrifuged at 4000 rpm for 3 min and the remaining precursors were washed several times with ethanol.

Step 3) Gold nanoparticle seeding: The pNE-coated $CsPbBr_3$ particles were mixed with 1 mL of ethanol solution containing colloidally dispersed PVP-functionalized 10 nm-sized gold nanoparticles (AuNPs) at a concentration of $\approx 4 \times 10^{12}$ AuNPs particles per mL. The solution was incubated on the vial shaker string at 1000 rpm for 12 h. Unbound gold nanoparticles were washed away by centrifugation at 4000 rpm for 3 min and using fresh ethanol solution.

Step 4) Gold film generation: The gold nanoparticle seeded $CsPbBr_3$ particles were immersed in 3.6 µM $KAuBr_4$ ethanol solution. For reducing the Au (III) ions, 1 µL of formaldehyde (38% H_2O) and 1 µL of NaOH (1N in H_2O) were added. The solution was stirred at 1000 rpm for 30 min at room temperature. The product was centrifuged at 4000 rpm for 3 min and the remaining precursors were washed several times with ethanol. Finally, the core–shell particles were stored in ethanol for further use.

Functionalization: For perovskite-lipid-bilayer hybrid, the large unilamellar vesicles (LUVs) consisting of DOPE and DOTAP were synthesized using a conventional extrusion method. Prepared LUVs in water were stained with DIR dye for near-infrared fluorescence imaging. For lipid-bilayer coating, the LUVs were mixed with pNE-coated $CsPbBr_3$ particles in ethanol in a 1:1 vol/vol ratio and then vortexed for 1 min for sufficient encapsulation. For red fluorescent protein coating, gold-coated $CsPbBr_3$ particles were mixed in PBS buffer containing rDSRed-express protein (100 µg mL^{-1}). After incubation for 5 min, the product was centrifuged at 8000 rpm for 5 min, and the supernatant was removed. The product was washed two times with fresh PBS to remove unattached proteins. The perovskite-RFP hybrid was re-dispersed in fresh PBS buffer and immediately transferred to a glass substrate for optical characterization.

Cell Experiment: The lipid-coated particles (concentration: 0.28 µg mL^{-1}) were added to live 4T1 breast cancer cells, and the cells were incubated at 37 °C and 5% CO_2 for 10 min. The cells were then stained after fixation with DAPI for nucleus. Particle uptake was confirmed using a fluorescence and bright-field microscope (Keyence BZ-X700 microscope).

Laser Experiments: A homebuilt epifluorescence microscope setup was used to characterize the optical properties of the core–shell particles (Figure S2, Supporting Information). The pump light source was an optical parametric oscillator (Opotek HE 355 LD) tuned to an output wavelength of 480 nm with a repetition rate of 20 kHz and a pulse duration of 4 ns. The pump light in a circular polarization state was focused on individual particles on a borosilicate substrate using a 0.9 NA, 100X air objective lens (Nikon) with a FWHM beam width of ≈25 µm. The output emission from a single particle was collected using the same objective lens, passed through a dichroic mirror and a dichroic filter, and split to an electron multiplication charge coupled device (EMCCD) camera (Luca, Andor) for wide-field imaging and to a grating-based EMCCD spectrometer (Shamrock, Andor) with a spectral resolution of ≈0.1 nm. For time-resolved photoluminescence (PL) measurements, a picosecond laser (VisIR-765, PicoQuant), frequency-doubled to 382 nm, was used for excitation. The detection modules consisted of a single-photon avalanche photodiode (Micro Photonics Devices) with a response time of 120 ps and a time-correlated single-photon counting board (TimeHarp 260, PicoQuant) with a resolution of 25 ps. For polarization measurement, a linear polarizer was placed on the detection path, and the polarizer angle was rotated using a motorized rotation mount. All optical measurements were conducted at room temperature.

Statistical Analysis: Data presentation, sample sizes (n), statistical analyses, and significance levels were detailed in the figure legends. Differences in the lasing stability of gold-coated $CsPbBr_3$ samples were assessed using MATLAB and are presented as mean ± standard deviation for $n = 8$, as specified in the legends.

Supporting Information

Supporting Information is available from the Wiley Online Library or from the author.

Acknowledgements

S.C. thanks Dr. Yoon-Ah Shin for helping in high-resolution TEM imaging and Dr. Yoonha Hwang for two-photon imaging and acknowledges the Bullock-Wellman fellowship award and the MGH Fund for Medical Discovery Fundamental Research fellowship award. This research was supported in part by funding from the National Institutes of Health (grants R01EB033155 and R01EB034687).

Conflict of Interest

S.H.Y. has financial interests in LASE Innovation Inc., a company focused on commercializing technologies based on laser particles that were reviewed and are managed by Massachusetts General Brigham in accordance with their conflict of-interest policies. All other authors declare no conflict of interest.

Author Contributions

S.C. and S.H.Y. designed the project. S.C. performed experiments and computer simulation. H.Y. assisted with cell experiments. S.C. and S.H.Y. wrote the manuscript with input from all authors.

Data Availability Statement

The data that support the findings of this study are available from the corresponding author upon reasonable request.

Keywords

biological imaging, laser, lead halide perovskite, metal coating, stability

Received: December 3, 2024
Revised: January 11, 2025
Published online:

[1] A. Fakharuddin, M. K. Gangishetty, M. Abdi-Jalebi, S.-H. Chin, A. R. bin Mohd Yusoff, D. N. Congreve, W. Tress, F. Deschler, M. Vasilopoulou, H. J. Bolink, *Nat. Electron.* **2022**, *5*, 203.
[2] J. Y. Kim, J.-W. Lee, H. S. Jung, H. Shin, N.-G. Park, *Chem. Rev.* **2020**, *120*, 7867.
[3] G. Xing, N. Mathews, S. S. Lim, N. Yantara, X. Liu, D. Sabba, M. Grätzel, S. Mhaisalkar, T. C. Sum, *Nat. Mater.* **2014**, *13*, 476.
[4] Y. Jia, R. A. Kerner, A. J. Grede, B. P. Rand, N. C. Giebink, *Nat. Photonics* **2017**, *11*, 784.

[5] H. Zhu, Y. Fu, F. Meng, X. Wu, Z. Gong, Q. Ding, M. V. Gustafsson, M. T. Trinh, S. Jin, X. Y. Zhu, *Nat. Mater.* **2015**, *14*, 636.
[6] S. Cho, M. Humar, N. Martino, S. H. Yun, *Phys. Rev. Lett.* **2016**, *117*, 193902.
[7] E. Tiguntseva, K. Koshelev, A. Furasova, P. Tonkaev, V. Mikhailovskii, E. V. Ushakova, D. G. Baranov, T. Shegai, A. A. Zakhidov, Y. Kivshar, *ACS Nano* **2020**, *14*, 8149.
[8] P. Geiregat, J. Maes, K. Chen, E. Drijvers, J. De Roo, J. M. Hodgkiss, Z. Hens, *ACS Nano* **2018**, *12*, 10178.
[9] S. Cho, Y. Yang, M. Soljačić, S. H. Yun, *Sci Adv.* **2021**, *7*, eabf3362.
[10] N. Martino, S. J. J. Kwok, A. C. Liapis, S. Forward, H. Jang, H.-M. Kim, S. J. Wu, J. Wu, P. H. Dannenberg, S.-J. Jang, Y.-H. Lee, S.-H. Yun, *Nat. Photonics* **2019**, *13*, 720.
[11] A. H. Fikouras, M. Schubert, M. Karl, J. D. Kumar, S. J. Powis, A. Di Falco, M. C. Gather, *Nat. Commun.* **2018**, *9*, 4817.
[12] D. Sarkar, S. Cho, H. Yan, N. Martino, P. H. Dannenberg, S. H. Yun, *ACS Nano* **2023**, *17*, 16048.
[13] S. J. J. Kwok, S. Forward, M. D. Fahlberg, E. R. Assita, S. Cosgriff, S. H. Lee, G. R. Abbott, H. Zhu, N. H. Minasian, A. S. Vote, N. Martino, S.-H. Yun, *Nat. Biomed. Eng.* **2024**, *8*, 310.
[14] S. Cho, N. Martino, S.-H. Yun, *Nat. Nanotechnol.* **2025**, *20*, https://doi.org/10.1038/s41565-024-01843-7.
[15] A. Dey, J. Ye, A. De, E. Debroye, S. K. Ha, E. Bladt, A. S. Kshirsagar, Z. Wang, J. Yin, Y. Wang, *ACS Nano* **2021**, *15*, 10775.
[16] L. Chouhan, S. Ghimire, C. Subrahmanyam, T. Miyasaka, V. Biju, *Chem. Soc. Rev.* **2020**, *49*, 2869.
[17] R. F. Oulton, V. J. Sorger, T. Zentgraf, R.-M. Ma, C. Gladden, L. Dai, G. Bartal, X. Zhang, *Nature* **2009**, *461*, 629.
[18] R.-M. Ma, R. F. Oulton, V. J. Sorger, G. Bartal, X. Zhang, *Nat. Mater.* **2011**, *10*, 110.
[19] Y.-J. Lu, J. Kim, H.-Y. Chen, C. Wu, N. Dabidian, C. E. Sanders, C.-Y. Wang, M.-Y. Lu, B.-H. Li, X. Qiu, *Science* **2012**, *337*, 450.
[20] Q. Zhang, G. Li, X. Liu, F. Qian, Y. Li, T. C. Sum, C. M. Lieber, Q. Xiong, *Nat. Commun.* **2014**, *5*, 4953.
[21] M. Khajavikhan, A. Simic, M. Katz, J. H. Lee, B. Slutsky, A. Mizrahi, V. Lomakin, Y. Fainman, *Nature* **2012**, *482*, 204.
[22] M. T. Hill, Y.-S. Oei, B. Smalbrugge, Y. Zhu, T. de Vries, P. J. van Veldhoven, F. W. M. van Otten, T. J. Eijkemans, J. P. Turkiewicz, H. de Waardt, E. J. Geluk, S.-H. Kwon, Y.-H. Lee, R. Nötzel, M. K. Smit, *Nat. Photonics* **2007**, *1*, 589.
[23] S. Yang, W. Bao, X. Liu, J. Kim, R. Zhao, R. Ma, Y. Wang, X. Zhang, *Matter* **2021**, *4*, 4042.
[24] E. V. Monaico, I. M. Tiginyanu, V. V. Ursaki, K. Nielsch, D. Balan, M. Prodana, M. Enachescu, *J. Electrochem. Soc.* **2017**, *164*, D179.
[25] C. Yilmaz, A. E. Cetin, G. Goutzamanidis, J. Huang, S. Somu, H. Altug, D. Wei, A. Busnaina, *ACS Nano* **2014**, *8*, 4547.
[26] F. Wang, S. Peters, J. Guzda, R. H. Blunk, A. P. Angelopoulos, *Langmuir* **2009**, *25*, 4384.
[27] S.-J. Cho, J.-C. Idrobo, J. Olamit, K. Liu, N. D. Browning, S. M. Kauzlarich, *Chem. Mater.* **2005**, *17*, 3181.
[28] B. Ji, E. Giovanelli, B. Habert, P. Spinicelli, M. Nasilowski, X. Xu, N. Lequeux, J.-P. Hugonin, F. Marquier, J.-J. Greffet, *Nat. Nanotechnol.* **2015**, *10*, 170.
[29] Y. Jin, X. Gao, *Nat. Nanotechnol.* **2009**, *4*, 571.
[30] R. A. Maniyara, D. Rodrigo, R. Yu, J. Canet-Ferrer, D. S. Ghosh, R. Yongsunthon, D. E. Baker, A. Rezikyan, F. J. García de Abajo, V. Pruneri, *Nat. Photonics* **2019**, *13*, 328.
[31] M. R. Hormozi Nezhad, M. Aizawa, L. A. Porter Jr, A. E. Ribbe, J. M. Buriak, *Small* **2005**, *1*, 1076.
[32] S. Y. Sayed, B. Daly, J. M. Buriak, *J. Phys. Chem. C* **2008**, *112*, 12291.
[33] L. Dou, M. Lai, C. S. Kley, Y. Yang, C. G. Bischak, D. Zhang, S. W. Eaton, N. S. Ginsberg, P. Yang, *Proc. Natl. Acad. Sci. USA* **2017**, *114*, 7216.
[34] G. Nedelcu, L. Protesescu, S. Yakunin, M. I. Bodnarchuk, M. J. Grotevent, M. V. Kovalenko, *Nano Lett.* **2015**, *15*, 5635.
[35] H. Zhu, S. Teale, M. N. Lintangpradipto, S. Mahesh, B. Chen, M. D. McGehee, E. H. Sargent, O. M. Bakr, *Nat. Rev. Mater.* **2023**, *8*, 569.
[36] R. Wang, M. Mujahid, Y. Duan, Z. Wang, J. Xue, Y. Yang, *Adv. Funct. Mater.* **2019**, *29*, 1808843.
[37] N. Li, X. Niu, Q. Chen, H. Zhou, *Chem. Soc. Rev.* **2020**, *49*, 8235.
[38] W. Xiang, S. F. Liu, W. Tress, *Energy Environ. Sci.* **2021**, *14*, 2090.
[39] S. Cho, Y. Yang, M. Soljačić´, S. H. Yun, *Nano Lett.* **2024**, *24*, 13647.
[40] Q. Zhong, M. Cao, H. Hu, D. Yang, M. Chen, P. Li, L. Wu, Q. Zhang, *ACS Nano* **2018**, *12*, 8579.
[41] X. Tang, W. Chen, Z. Liu, J. Du, Z. Yao, Y. Huang, C. Chen, Z. Yang, T. Shi, W. Hu, *Small* **2019**, *15*, 1900484.
[42] S. Li, D. Lei, W. Ren, X. Guo, S. Wu, Y. Zhu, A. L. Rogach, M. Chhowalla, A. K.-Y. Jen, *Nat. Commun.* **2020**, *11*, 1.
[43] H. Liu, Y. Tan, M. Cao, H. Hu, L. Wu, X. Yu, L. Wang, B. Sun, Q. Zhang, *ACS Nano* **2019**, *13*, 5366.
[44] X. Liu, X. Zhang, L. Li, J. Xu, S. Yu, X. Gong, J. Zhang, H. Yin, *ACS Appl. Mater. Interfaces* **2019**, *11*, 40923.
[45] Z. Li, E. Hofman, J. Li, A. H. Davis, C. Tung, L. Wu, W. Zheng, *Adv. Funct. Mater.* **2018**, *28*, 1704288.
[46] Y.-M. Chen, Y. Zhou, Q. Zhao, J.-Y. Zhang, J.-P. Ma, T.-T. Xuan, S.-Q. Guo, Z.-J. Yong, J. Wang, Y. Kuroiwa, *ACS Appl. Mater. Interfaces* **2018**, *10*, 15905.
[47] S. Cho, S. H. Yun, *Commun. Chem.* **2020**, *3*, 15.
[48] S. Cho, S. H. Yun, *Adv. Funct. Mater.* **2021**, *31*, 2101902.
[49] Y. Kwon, S. C. S. Lai, P. Rodriguez, M. T. M. Koper, *J. Am. Chem. Soc.* **2011**, *133*, 6914.
[50] P. Anger, P. Bharadwaj, L. Novotny, *Phys. Rev. Lett.* **2006**, *96*, 113002.
[51] Z. Wang, X. Meng, S. H. Choi, S. Knitter, Y. L. Kim, H. Cao, V. M. Shalaev, A. Boltasseva, *Nano Lett.* **2016**, *16*, 2471.
[52] X. Zheng, J. Zhang, J. Wang, X. Qi, J. M. Rosenholm, K. Cai, *J. Phys. Chem. C* **2015**, *119*, 24512.
[53] X. Huang, H. Li, C. Zhang, S. Tan, Z. Chen, L. Chen, Z. Lu, X. Wang, M. Xiao, *Nat. Commun.* **2019**, *10*, 1.
[54] N. Ahn, K. Kwak, M. S. Jang, H. Yoon, B. Y. Lee, J.-K. Lee, P. V. Pikhitsa, J. Byun, M. Choi, *Nat. Commun.* **2016**, *7*, 13422.
[55] V. M. Titze, S. Caixeiro, A. Di Falco, M. Schubert, M. C. Gather, *ACS Photonics* **2022**, *9*, 952.
[56] S. H. Yun, S. J. J. Kwok, *Nat. Biomed. Eng.* **2017**, *1*, 8.
[57] H. Yu, X. Xu, H. Liu, Y. Wan, X. Cheng, J. Chen, Y. Ye, L. Dai, *ACS Nano* **2019**, *14*, 552.
[58] S. Huang, Z. Shen, Y. Liao, Z. Liu, Z. Hu, Q. Li, Z. Zhang, S. Dong, J. Luo, J. Du, *Adv. Mater.* **2023**, *35*, 2306102.
[59] S. K. Avugadda, A. Castelli, B. Dhanabalan, T. Fernandez, N. Silvestri, C. Collantes, D. Baranov, M. Imran, L. Manna, T. Pellegrino, *ACS Nano* **2022**, *16*, 13657.
[60] H. Zhang, X. Wang, Q. Liao, Z. Xu, H. Li, L. Zheng, H. Fu, *Adv. Funct. Mater.* **2017**, *27*, 1604382.
[61] W. Song, D. Wang, J. Tian, G. Qi, M. Wu, S. Liu, T. Wang, B. Wang, Y. Yao, Z. Zou, *Small* **2022**, *18*, 2204763.
[62] Y. Yue, H. Xu, L. Jiang, X. Zhao, D. Deng, *Adv. Healthcare Mater.* **2023**, *13*, 2302721.
[63] Z. Yang, S. Zong, K. Yang, K. Zhu, N. Li, Z. Wang, Y. Cui, *ACS Appl. Mater. Interfaces* **2022**, *14*, 17109.
[64] E. Krauss, R. Kullock, X. Wu, P. Geisler, N. Lundt, M. Kamp, B. Hecht, *Cryst. Growth Des.* **2018**, *18*, 1297.
[65] X. Cauchy, J.-E. Klemberg-Sapieha, D. Therriault, *ACS Appl. Mater. Interfaces* **2017**, *9*, 29010.
[66] B. S. Gillis, Z. Arbieva, I. M. Gavin, *BMC Genomics* **2012**, *13*, 344.
[67] A. Babayigit, D. Duy Thanh, A. Ethirajan, J. Manca, M. Muller, H.-G. Boyen, B. Conings, *Sci. Rep.* **2016**, *6*, 18721.
[68] Y. Li, H. Zhou, M. Xia, H. Shen, T. Wang, H. Gao, X. Sheng, Y. Han, Z. Chen, L. Dou, *Sci. Adv.* **2023**, *9*, eadh0517.

[69] A. Babayigit, A. Ethirajan, M. Muller, B. Conings, *Nat. Mater.* **2016**, *15*, 247.
[70] L. Xiao, T. An, C. Deng, X. Xu, H. Sun, *Energy Environ. Sci.* **2023**, *16*, 2120.
[71] L. Lanzetta, N. Aristidou, S. A. Haque, *J. Phys. Chem. Lett.* **2020**, *11*, 574.
[72] I. Spanopoulos, I. Hadar, W. Ke, P. Guo, S. Sidhik, M. Kepenekian, J. Even, A. D. Mohite, R. D. Schaller, M. G. Kanatzidis, *J. Am. Chem. Soc.* **2020**, *142*, 9028.
[73] I. Park, L. Chu, K. Leng, Y. F. Choy, W. Liu, I. Abdelwahab, Z. Zhu, Z. Ma, W. Chen, Q. Xu, *Adv. Funct. Mater.* **2019**, *29*, 1904810.
[74] T. J. Macdonald, L. Lanzetta, X. Liang, D. Ding, S. A. Haque, *Adv. Mater.* **2023**, *35*, 2206684.
[75] X. Li, J. M. Hoffman, M. G. Kanatzidis, *Chem. Rev.* **2021**, *121*, 2230.
[76] J. Jang, Y. Kim, S. Park, D. Yoo, H. Cho, J. Jang, H. B. Jeong, H. Lee, J. M. Yuk, C. B. Park, *Adv. Mater.* **2021**, *33*, 2005255.
[77] M. Li, D. Yang, X. Huang, H. Zhang, Y. Zhao, B. Yin, Q. Pan, J. Kang, N. Zheng, X. Liu, *Adv. Mater.* **2022**, *34*, 2201413.
[78] X. Huang, Q. Guo, D. Yang, X. Xiao, X. Liu, Z. Xia, F. Fan, J. Qiu, G. Dong, *Nat. Photonics* **2020**, *14*, 82.
[79] C. Qin, A. S. D. Sandanayaka, C. Zhao, T. Matsushima, D. Zhang, T. Fujihara, C. Adachi, *Nature* **2020**, *585*, 53.
[80] W. Shao, J. H. Kim, J. Simon, Z. Nian, S.-D. Baek, Y. Lu, C. B. Fruhling, H. Yang, K. Wang, J. Y. Park, *Science* **2024**, *384*, 1000.
[81] G. Li, J. Tao, Z. Hou, K. Zhao, R. Zhao, T. Ji, Q. Zhang, Q. Xiong, K. Zheng, T. Pullerits, *Adv. Funct. Mater.* **2024**, *34*, 2405559.
[82] J. J. Baumberg, J. Aizpurua, M. H. Mikkelsen, D. R. Smith, *Nat. Mater.* **2019**, *18*, 668.
[83] P. A. D. Gonçalves, T. Christensen, N. Rivera, A.-P. Jauho, N. A. Mortensen, M. Soljačić, *Nat. Commun.* **2020**, *11*, 366.